PERGAMON

International Journal of Heat and Mass Transfer 44 (2001) 3223–3231

International Journal of HEAT and MASS TRANSFER

www.elsevier.com/locate/ijhmt

Optimal shape and arrangement of staggered pins in the channel of a plate heat exchanger

Kwan-Soo Lee *, Woo-Seung Kim, Jong-Min Si

School of Mechanical Engineering, Hanyang University, 17 Haengdang-dong, Sungdong-ku, Seoul 133-791, South Korea

Received 21 July 2000; received in revised form 27 October 2000

Abstract

The optimum shape and arrangement of staggered pins in the channel of a plate heat exchanger are studied in this paper. The following four dimensionless geometric parameters of the pins are selected as the important design variables: the distance (**L**), the volume (**V**), the angle (**β**) and the pitch (**G**). The pressure drop and heat transfer characteristics are examined, and an optimization is carried out to minimize a global objective function consisting of the correlation between the Nusselt number and the friction factor. The optimal geometric parameters are as follows: $\mathbf{L} = 0.272$, $\mathbf{V} = 0.106$, $\boldsymbol{\beta} = 0.44$ and $\mathbf{G} = 0.195$. The optimal geometric parameters obtained from this study can be applied for a Reynolds number ranging from 500 to 1500.

1. Introduction

Heat exchangers have to be installed in confined space of transport vehicles such as automobiles and aircrafts, or in otherwise "small" cooling packages: therefore, plate heat exchangers have been widely employed in the cooling systems for their compact size and high performance. In general, the flow passages of a compact plate heat exchanger are characterized by a small hydraulic diameter (few millimeters) and low velocity (less than 1 m/s). Hence, the flow is laminar for the most range of their operation. Among the techniques to enhance their thermal and flow performance, protrusions such as ribs and pins attached to the inner wall are very useful because they do not increase the total volume of the heat exchanger. Protrusions generate flow deflection and secondary flows by disturbing the through-flow and breaking the thermal boundary layers. Therefore, not only the heat transfer but also the pressure drop is increased. It is thus required to look for the optimal protrusion shape and arrangement that augment the heat transfer with the minimal pressure drop penalty. In the case of plate heat exchangers with protrusions, however, many arbitrarily-shaped protrusions are present, and it looks almost impossible to analyze the entire geometry numerically because too many grid points would be required. The geometry considered in the present analysis varies in a periodic manner along the direction of the flow. The concept of a periodic fully developed regime can be employed in the analysis of these periodic geometries [1].

Many works [1–6] have been reported on the thermal and flow performance and optimization in the channels with protrusions. Choudhury and Karki [1] have numerically analyzed a fully developed flow and heat transfer in streamwise-periodic dimpled channels for two-dimensional laminar flow. Ohara et al. [2] have experimentally examined the characteristics of the heat transfer and pressure drop at height and spacing of repeated transverse ribs in a channel. Fowler et al. [3] have predicted the optimal geometric arrangement of staggered plates to maximize heat transfer under external forced convection. However, studies related to the effect of geometric parameters of pins on the thermal and flow performance at low Reynolds number and channel with high aspect ratio are very scant, though it is the most practical case.

In the present work, the thermal and flow performance in the channel of a plate heat exchanger with

* Corresponding author. Tel.: +82-2-2290-0426; fax: +82-2-2295-9021.

E-mail address: ksleehy@email.hanyang.ac.kr (K.-S. Lee).

0017-9310/01/$ - see front matter
PII: S0017-9310(00)00350-1

Nomenclature

A	heat transfer area of smooth parallel plate channel (without pins) (m^2)
B	overall pressure gradient
D_1	pin diameter at the symmetric plane (m)
D_2	pin diameter at the lower plane (m)
D_h	hydraulic diameter (m)
f	friction factor
$F(x)$	global objective function
$g(x)$	a curve-fitting function
G	pin pitch (m)
G	dimensionless pin pitch
h	average heat transfer coefficient (W/m^2 K)
L	pin spacing (m)
L	dimensionless pin spacing
Nu	average Nusselt number
P	local pressure (N/m^2)
Pr	Prandtl number, v/α
Q	heat transfer rate in the computational domain (W)
Re	Reynolds number, $\bar{v}D_h/v$
T	temperature (°C)
u, v, w	velocity components (m/s)
$\bar{v}$	average inlet velocity (m/s)
V	pin volume (m^3)
V	dimensionless pin volume
x, y, z	Cartesian coordinates
X	width of the computational domain (m)
X	a vector of design variables
Y	length of the computational domain (m)
Z	height of the computational domain (m)

Greek symbols

β	pin angle (°)
β	dimensionless pin angle
θ	dimensionless temperature, Eq. (9)
ρ	fluid density (kg/m^3)
ϕ	dimensionless temperature, Eq. (11)

Subscripts

0	smooth parallel plate channel (i.e., without pins)
b	bulk value
w	value at the channel wall
opt	optimum value
max	maximum value
base	baseline model

pins is analyzed in a three-dimensional, periodic, fully-developed laminar regime. An optimized geometry of the pins is found by maximizing the thermal performance.

2. Theoretical analysis

The geometry considered in this study is shown in Fig. 1. Since Fig. 1 has repetitive pin arrangements, it is assumed that the computational domain can be restricted to a typical module shown in Fig. 2 [1]. Pin spacing (L), pin volume (V), pin angle (β) and pin pitch (G) are chosen as the most important geometric parameters, and their dimensionless forms are defined as

$$\mathbf{L} = \frac{L}{X}, \quad \mathbf{V} = \frac{V}{V_0}, \quad \boldsymbol{\beta} = \frac{\beta}{\beta_{\max}}, \quad \mathbf{G} = \frac{G}{X}, \tag{1}$$

where $\beta_{\max}$ is 90° and V_0 is the fluid volume of the smooth parallel plate channel (i.e., without pins). A baseline model is taken from a commercial plate heat exchanger and its dimensions are given in Table 1. To analyze the thermal and flow characteristics of this model, the following assumptions are made:

1. The flow is three-dimensional, steady-state, incompressible and laminar.
2. The channel walls and pins are kept at constant temperature.
3. The flow pattern in the streamwise direction is periodic and fully developed.
4. The effects of body force and buoyancy are neglected.

The pressure p in the periodic fully developed flow can be expressed as [7]

$$p(x, y, z) = -By + P(x, y, z), \tag{2}$$

where B is a constant representing the overall pressure gradient and the local pressure (P) has a periodicity as follows:

$$P(x, y, z) = P(x, y + Y, z). \tag{3}$$

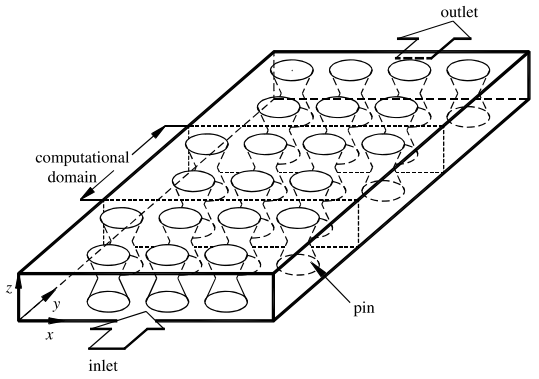

Fig. 1. Schematic diagram of the physical model.

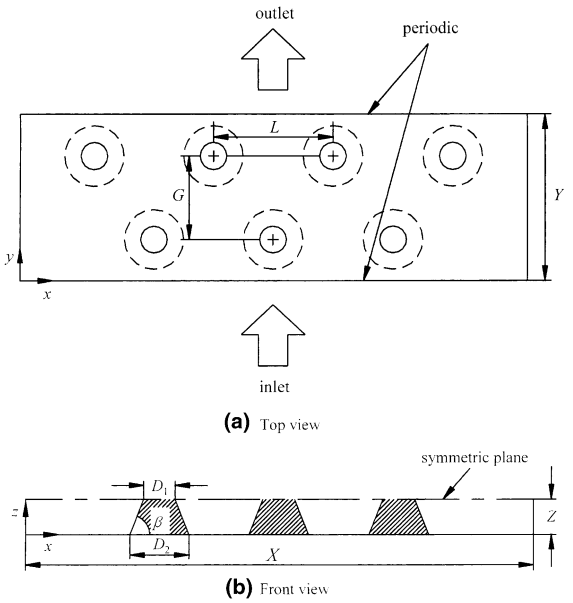

Fig. 2. Schematic diagram of the computational domain.

Table 1
Geometric parameters of the baseline model

Geometric parameter	Dimension
X (width of the channel)	31.00 mm
Y (length of the channel)	12.12 mm
Z (height of the channel)	0.98 mm
L (pin spacing)	7.00 mm
G (pin pitch)	6.06 mm
β (pin angle)	39.2°
D_1 (pin diameter at the symmetric plane)	1.40 mm
D_2 (pin diameter at the bottom)	3.80 mm

The governing equations based on the above assumptions are as follows:

$$\frac{\partial u}{\partial x}+\frac{\partial v}{\partial y}+\frac{\partial w}{\partial z}=0, \tag{4}$$

$$\rho\left(u\frac{\partial u}{\partial x}+v\frac{\partial u}{\partial y}+w\frac{\partial u}{\partial z}\right)=-\frac{\partial P}{\partial x}+\mu\left(\frac{\partial^2 u}{\partial x^2}+\frac{\partial^2 u}{\partial y^2}+\frac{\partial^2 u}{\partial z^2}\right), \tag{5}$$

$$\rho\left(u\frac{\partial v}{\partial x}+v\frac{\partial v}{\partial y}+w\frac{\partial v}{\partial z}\right)=B-\frac{\partial P}{\partial y}+\mu\left(\frac{\partial^2 v}{\partial x^2}+\frac{\partial^2 v}{\partial y^2}+\frac{\partial^2 v}{\partial z^2}\right), \tag{6}$$

$$\rho\left(u\frac{\partial w}{\partial x}+v\frac{\partial w}{\partial y}+w\frac{\partial w}{\partial z}\right)=-\frac{\partial P}{\partial z}+\mu\left(\frac{\partial^2 w}{\partial x^2}+\frac{\partial^2 w}{\partial y^2}+\frac{\partial^2 w}{\partial z^2}\right), \tag{7}$$

$$u\frac{\partial T}{\partial x}+v\frac{\partial T}{\partial y}+w\frac{\partial T}{\partial z}=\alpha\left(\frac{\partial^2 T}{\partial x^2}+\frac{\partial^2 T}{\partial y^2}+\frac{\partial^2 T}{\partial z^2}\right). \tag{8}$$

When the thermal boundary conditions are either uniform wall temperature or uniform wall heat flux, the temperature field becomes periodic. Thus, a periodic dimensionless temperature is defined as

$$\theta(x,y,z)=\frac{T(x,y,z)-T_{\mathrm{w}}}{T_{\mathrm{b}}(y)-T_{\mathrm{w}}}, \tag{9}$$

where

$$T_{\mathrm{b}}(y)=\frac{\int_0^X\int_0^Z |v|T\,\mathrm{d}z\,\mathrm{d}x}{\int_0^X\int_0^Z |v|\,\mathrm{d}z\,\mathrm{d}x}, \tag{10}$$

where T_{w} is the wall temperature and $T_{\mathrm{b}}(y)$ indicates the bulk temperature. To further facilitate the analysis, a new dimensionless temperature ϕ related to θ is defined as [8]

$$\phi(x,y,z)=\frac{T(x,y,z)-T_{\mathrm{w}}}{T_{\mathrm{b}}(0)-T_{\mathrm{w}}}. \tag{11}$$

The energy equation (8) can be expressed in terms of ϕ as

$$u\frac{\partial \phi}{\partial x}+v\frac{\partial \phi}{\partial y}+w\frac{\partial \phi}{\partial z}=\alpha\left(\frac{\partial^2 \phi}{\partial x^2}+\frac{\partial^2 \phi}{\partial y^2}+\frac{\partial^2 \phi}{\partial z^2}\right). \tag{12}$$

The boundary conditions at the upper and lower walls, and the periodic boundaries are given as:

- at all the walls and pin surfaces

  $u=v=w=0, \quad \phi=0,$

- at the symmetric surface $(z=Z)$

  $\partial u/\partial z=0, \quad \partial v/\partial z=0, \quad w=0, \quad \partial \phi/\partial z=0,$

- at the periodic boundaries $(y=0, y=Y)$

  $u(x,0,z)=u(x,Y,z),$
  $v(x,0,z)=v(x,Y,z),$
  $w(x,0,z)=w(x,Y,z),$
  $\phi(x,0,z)=\phi(x,Y,z)/\phi_{\mathrm{b}}(Y),$

  where $\phi_{\mathrm{b}}(Y)$ is defined as

$$\phi_{\mathrm{b}}(Y)=\frac{\int_0^X\int_0^Z |v|\phi\,\mathrm{d}z\,\mathrm{d}x}{\int_0^X\int_0^Z |v|\,\mathrm{d}z\,\mathrm{d}x}. \tag{13}$$

The solution of the flow field was obtained by following the procedure suggested in [1].

The friction factor is defined as

$$f=\frac{BD_{\mathrm{h}}}{\rho\overline{v}^2/2}, \tag{14}$$

where the average velocities $\overline{v}$ and the hydraulic diameter D_h are given by

$$\overline{v} = \frac{\int_0^X \int_0^Z v \, dz \, dx}{XZ}, \tag{15}$$

$$D_h = 8XZ/2(X + 2Z) \cong 4Z. \tag{16}$$

The overall heat transfer performance can be estimated by the average Nusselt number given as

$$Nu = \frac{hD_h}{k}, \tag{17}$$

where the average heat transfer coefficient h is defined as

$$h = \frac{Q}{A \cdot \mathrm{LMTD}}, \tag{18}$$

where A represents heat transfer area of the smooth parallel plate channel (i.e., without pins), and Q indicates the total rate of heat transfer in the computational domain given by

$$Q = \rho \overline{v} XZ c_p (T_b(0) - T_b(Y)). \tag{19}$$

The log-mean temperature difference LMTD is defined as

$$\mathrm{LMTD} = \frac{(T_w - T_b(Y)) - (T_w - T_b(0))}{\ln[(T_w - T_b(Y))/(T_w - T_b(0))]}. \tag{20}$$

3. Grid generation and numerical analysis

In the present study, a partial differential method is used to generate the grids. This method has a drawback since it cannot handle arbitrary geometries such as pins in a computational domain. Hence, as shown in Figs. 3(a) and (b), the computational domain is divided into nine sub-domains and each sub-domain is also composed of nine end-domains. The grids are generated at each end-domain and then combined into one grid system. To prevent the occurrence of the discontinuous grid points at the interfaces between end-domains, the grids are readjusted to be smooth at the adjacent boundary surfaces. Since pin diameter changes along the z-direction, the grid generated with varying pin diameter is laminated to the z-direction. The cross-section of the grid system generated by using the present method is shown in Fig. 3(c). The grid dependence test has been performed by changing the number of grid points. The grid system used in the present model is $85 \times 43 \times 15$ by considering that the changes of module Nusselt number and friction factor are both less than 2%.

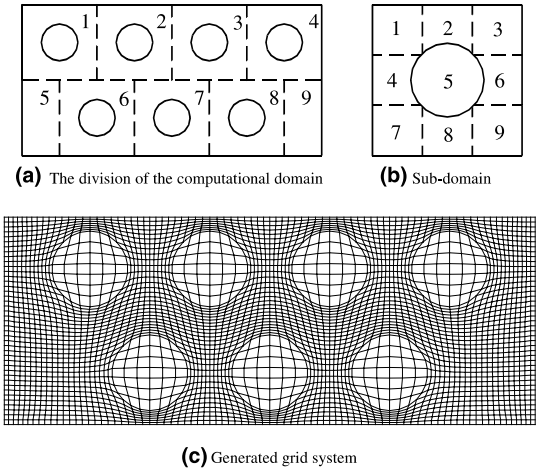

Fig. 3. Grid system used in this study.

A finite difference method is applied to discretize the governing equations. A second-order central differencing scheme and adaptive second- and fourth-order dissipation terms are used to compute the convective terms. The adaptive damping terms are constructed in such a way that a fourth-order damping scheme is activated in the smooth regions, and a second-order damping scheme is used in the domains with high gradient of physical properties. Second-order central differencing scheme is used for the viscous and the source terms. The diffusion terms are divided into orthogonal and non-orthogonal terms. The orthogonal terms are treated implicitly and the non-orthogonal terms are lumped in the explicit part of the source terms. A pressure-based predictor/multi-corrector solution procedure is employed to ensure velocity–pressure coupling and divergence-free flow field solutions. A first-order upwind scheme is employed for all scalar transport equations. To solve for the steady-state solution, an implicit Euler time marching scheme is applied.

When the rates of maximum change in the velocity and temperature field are smaller than 10^{-6} and the values of μ's in all calculation domains are not changed, the results are considered to be converged. It is not certain whether there is any unsteadiness in the flow at the given Reynolds number 1000 based on the hydraulic diameter of the channel. For flow past a cylinder with a bounding wall, unsteady oscillation as well as horseshoe vortices appear at this Reynolds number. In our case, however, the bounding upper and lower walls, together with the hollow pin waist, maintain steady laminar flow to a greater Reynolds number. Since no experimental observation has been made, the only verification may check the numerical false diffusion [9]. Note that the scheme employed here uses a relaxation factor for each variable, which is a pseudo-unsteady scheme. Consequently, if the flow is actually oscillatory and the scheme is free from false diffusion, the numerical convergence also exhibits oscillatory fashion and convergence may not be achieved after all. We check the maximum false

diffusion coefficient following the two-dimensional results of de Vahl Davis and Mallinson [10] at each layer in the z-direction. No oscillatory convergence is observed. These two evidences may be taken as the clue to the justification of the employed numerical scheme for laminar steady flow. A complete proof, however, should be made via an experimental study.

4. Parametric studies

The results are presented in terms of the two ratios, Nu/Nu_0 and $fRe/(fRe)_0$, where the subscript 0 refers to a smooth parallel plate channel without pins. The values of Nu_0 and $(fRe)_0$ are 7.54 and 96, respectively [11]. The effect of each geometric parameter has been examined with $Re = 1000$ and $Pr = 4$, which are typical values of the operating parameters of the baseline model used in this study.

4.1. Effect of various parameters

Fig. 4 shows the values of Nu/Nu_0 and $fRe/(fRe)_0$ from the baseline model at $Pr = 4$ as a function of the Reynolds number. It indicates that both the Nusselt number and the friction factor increase with the Reynolds number. This may be attributed to the fact that increasing the Reynolds number amplifies flow distortion due to the pins; thus, the increase of the effect of flow distortion caused by pins yields an increase of heat transfer and pressure drop. This can also be shown in Figs. 5(a) and (b) which represent the thermal and flow field at the symmetric plane $(z = Z)$ of the baseline model. For $Re = 100$, there is little effect of flow distortion due to the pins on the heat transfer and pressure drop because of slow velocity. Increasing the Reynolds number causes the size of recirculation zone at the back surface of the pin to grow. The influence of flow impingement against the front surface of the pins is also increased. Hence, the heat transfer rate and pressure drop increase significantly.

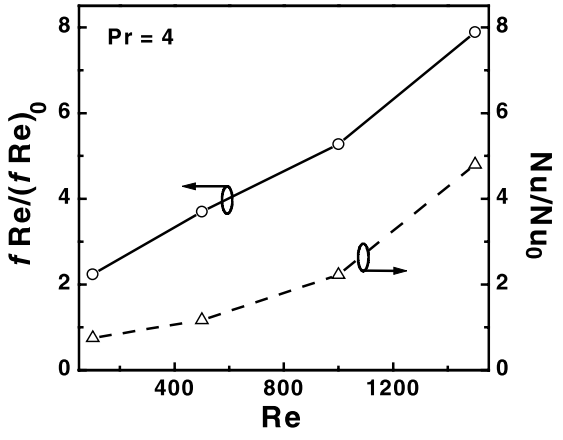

Fig. 4. The ratios of friction factor and Nusselt number vs Reynolds number.

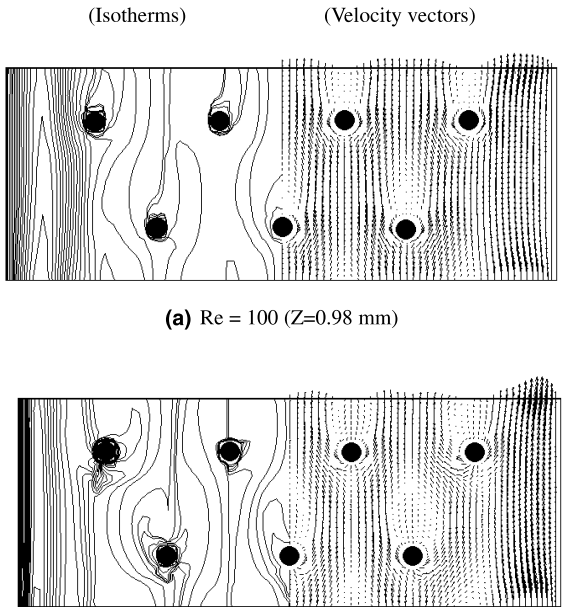

Fig. 5. Isotherms and velocity vectors in the channel with pins (•: pin).

Parametric studies of geometric parameters have also been carried out to determine the degree of importance of each parameter. They have been conducted by analyzing the thermal and flow characteristics, varying only one parameter among the baseline parameters.

Fig. 6 shows the variations of $fRe/(fRe)_0$ and Nu/Nu_0 as a function of the dimensionless pin spacing. For a small value of **L**, most of the flow passes through the left and right ends of the channel (see Fig. 2) due to the small width of the flow passages between the pins. However, as **L** increases, more fluid flows through the passage between the pins rather than both ends of the channel. With increasing **L**, the increase of flow distortion due to the impingement against the pins increases the heat transfer rate and the pressure drop.

Fig. 7 shows the ratios of the friction factor and the Nusselt number as a function of the volume of the pin. As **V** increases, blockage effect is increased due to the reduction of flow cross-section area and thus, the effect of flow impingement against pins is increased. The heat transfer enhancement and pressure drop tend to be increased.

Fig. 8 shows the ratios of the friction factor and the Nusselt number as a function of the pin angle. It is

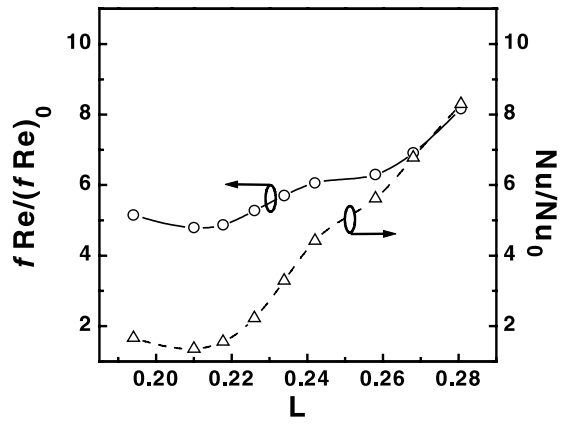

Fig. 6. The ratios of friction factor and Nusselt number vs pin spacing.

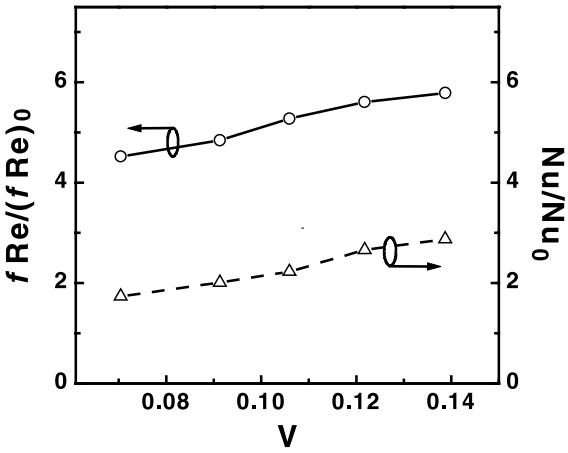

Fig. 7. The ratios of friction factor and Nusselt number vs pin volume.

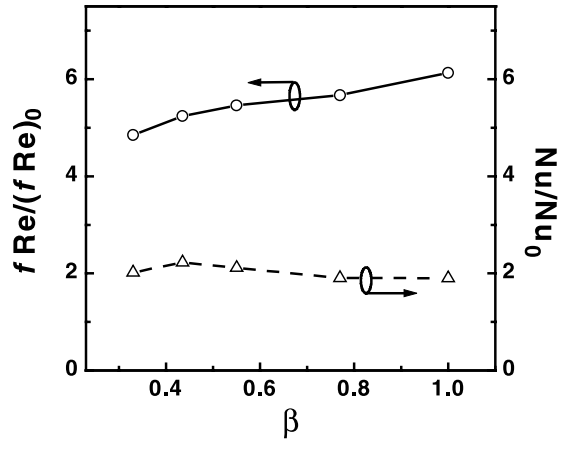

Fig. 8. The ratios of friction factor and Nusselt number vs pin angle.

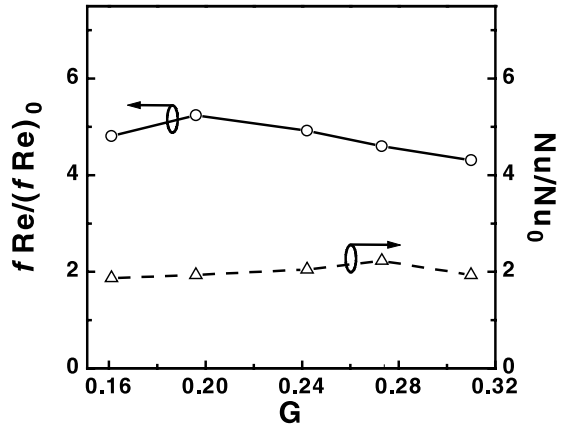

Fig. 9. The ratios of friction factor and Nusselt number vs pin pitch.

considered that each pin contains the same volume in the channel. As **β** increases, a separation point moves towards the front face of the pin and thus, the size of the recirculation zone develops and a vortex is observed near the bottom of the pin. Hence, pressure drop increases due to the increase of the drag from the recirculation zone and vortex. The total surface area of pin is decreased, however, the enhancement of the heat transfer rate is observed due to the increase of the bottom area and the vortex near the bottom of the pin. However, Fig. 8 indicates that the heat transfer rate for the values of **β** greater than 0.5 decreases slowly. This results from the fact that the effect of decreasing the surface area of the pin is larger.

Fig. 9 shows the ratios of the friction factor and the Nusselt number as a function of the pin pitch. It is seen that for very small values of **G**, heat transfer enhancement and pressure drop are relatively small because most of the flow passes through the left and right ends of the channel as in the case of the small values of **L**. As **G** increases, heat transfer enhancement and pressure drop increase due to the effect of flow distortion and recirculation zone generated in the increased space between the rows. However, when **G** is greater than about 0.2, pressure drop decreases because the effects due to recirculation zone and flow distortion decrease with further increase of **G**. Although heat transfer increases up to about 0.28, its variation is not significant.

4.2. Importance of geometric parameters

Table 2 shows the maximum and the minimum values of the two ratios, Nu/Nu_0 and $fRe/(fRe)_0$, among the results of the parametric studies performed in the previous section. The degree of importance of the parameters is determined based on the magnitude of the differences for each ratio in Table 2. It resulted in

Table 2
The result of parameter studies

Parameters	Range	fRe/fRe_0		Difference	Nu/Nu_0		Difference
		Max	Min		Max	Min	
L	0.194–0.280	8.16	4.79	3.37	8.30	1.35	6.95
V	0.070–0.138	5.81	4.53	1.28	2.87	1.73	1.14
β	0.33–1.00	6.13	4.95	1.18	2.23	1.9	0.33
G	0.161–0.310	5.24	4.31	0.93	2.1	1.87	0.23

the order of **L**, **V**, **β**, and **G** for both ratios. It shows that **L** is the most effective parameter to the thermal and flow performance because its difference between the maximum and minimum values of each ratio is over three times greater than that of the other parameters.

5. Optimization

In order to enhance thermal and flow characteristics in the channel of a plate heat exchanger with pins, the following two performance requirements are considered:

- to minimize the pressure drop,
- to maximize the heat transfer.

Denoting a vector of the design variables (**L**, **V**, **β**, **G**) as **X**, a multi-objective optimization problem can be formulated as follows: find the design variable vector **X** to

$$\text{minimize} \quad \begin{Bmatrix} Nu_0/Nu \\ fRe/(fRe)_0 \end{Bmatrix}, \tag{21}$$

$$\text{subject to} \quad \mathrm{X}_k^{\mathrm{L}} \leqslant \mathrm{X}_k \leqslant \mathrm{X}_k^{\mathrm{U}}, \quad k = 1,2,3,4. \tag{22}$$

Note that the inverse of Nusselt number is used in Eq. (21) to maximize Nusselt number.

Optimization is sequentially carried out in the order of the importance of parameters obtained in Table 2. Hence the above problem can be reduced to a single variable optimization problem. The correlations of the two ratios, Nu/Nu_0 and $fRe/(fRe)_0$, are determined by using curve-fitting to keep the coefficient of determination above 0.99 in the heat and fluid flow analysis for each geometric parameter. They are denoted by $g_1(x)$ and $g_2(x)$, respectively. A global criterion function $F(x)$ is determined by using the global criterion method proposed by Rio [12] to simultaneously consider the effects of these two functions. Therefore, Eqs. (21) and (22) are converted as follows: find the design variable x to

$$\text{minimize} \quad F(x) = \sum_{i=1}^{2} \left\{ \frac{g_i(x_i^*) - g_i(x)}{g_i(x_i^*)} \right\}^2, \tag{23}$$

$$\text{subject to} \quad x^{\mathrm{L}} \leqslant x \leqslant x^{\mathrm{U}}, \tag{24}$$

where x_i^* is obtained by minimizing $g_1(x)$ and $g_2(x)$ under the constraints. The augmented Lagrange multiplier (ALM) method is employed to minimize the global criterion function expressed by Eq. (23) under the constraint given by Eq. (24). Broyden–Fletcher–Goldfarb–Shanno (BFGS) method is used to search for the decreasing direction, and the golden section method is applied for line search.

Fig. 10 shows the optimization procedure used in this study. First, the most important parameter **L** is optimized. Then optimization is performed in the order of **V**, **β** and **G**. Other parameters except **L** are changed by about ±20–30% from the original values, and optimum values are obtained for five cases as shown in Table 3. If the values of the global criterion function of Case A are larger than those of the other cases, the parameters with the smallest values of the global criterion function are selected as a new baseline model and optimization procedure is repeated again.

To obtain the optimum values of the parameters, computational analysis of thermal and flow characteristics has been carried out about 100 times. An optimum model is defined by using the optimum parameters obtained from the above procedures, and then the values of the two ratios, Nu/Nu_0 and $fRe/(fRe)_0$, are determined from the optimum model. The optimum values for each parameter and the ratios, Nu/Nu_0 and $fRe/(fRe)_0$, from the optimum model are presented in Tables 4 and 5, respectively. The optimization procedure has also been performed by varying the order of **V**, **β** and **G**, since the differences between the maximum and minimum values of each ratio are not noticeable for these three parameters. It is interesting to note that all cases yielded the same results as shown in Table 4. This may result from the fact that the optimum values of **V**, **β** and **G** are not quite different from their values of the baseline model.

Until now, the Reynolds number has been set to 1000. However, various values of Reynolds number ranging from 500 to 1500 have also been considered in the analysis, and the variations of $\mathbf{L}_{\mathrm{opt}}$ and $\boldsymbol{\beta}_{\mathrm{opt}}$ as a function of the Reynolds number are represented in Fig. 11. As shown in the graph, there are little differences in the values of $\mathbf{L}_{\mathrm{opt}}$ and $\boldsymbol{\beta}_{\mathrm{opt}}$. Therefore, the optimum geometric parameters obtained from this study can be applied to the Reynolds number ranging from 500 to 1500.

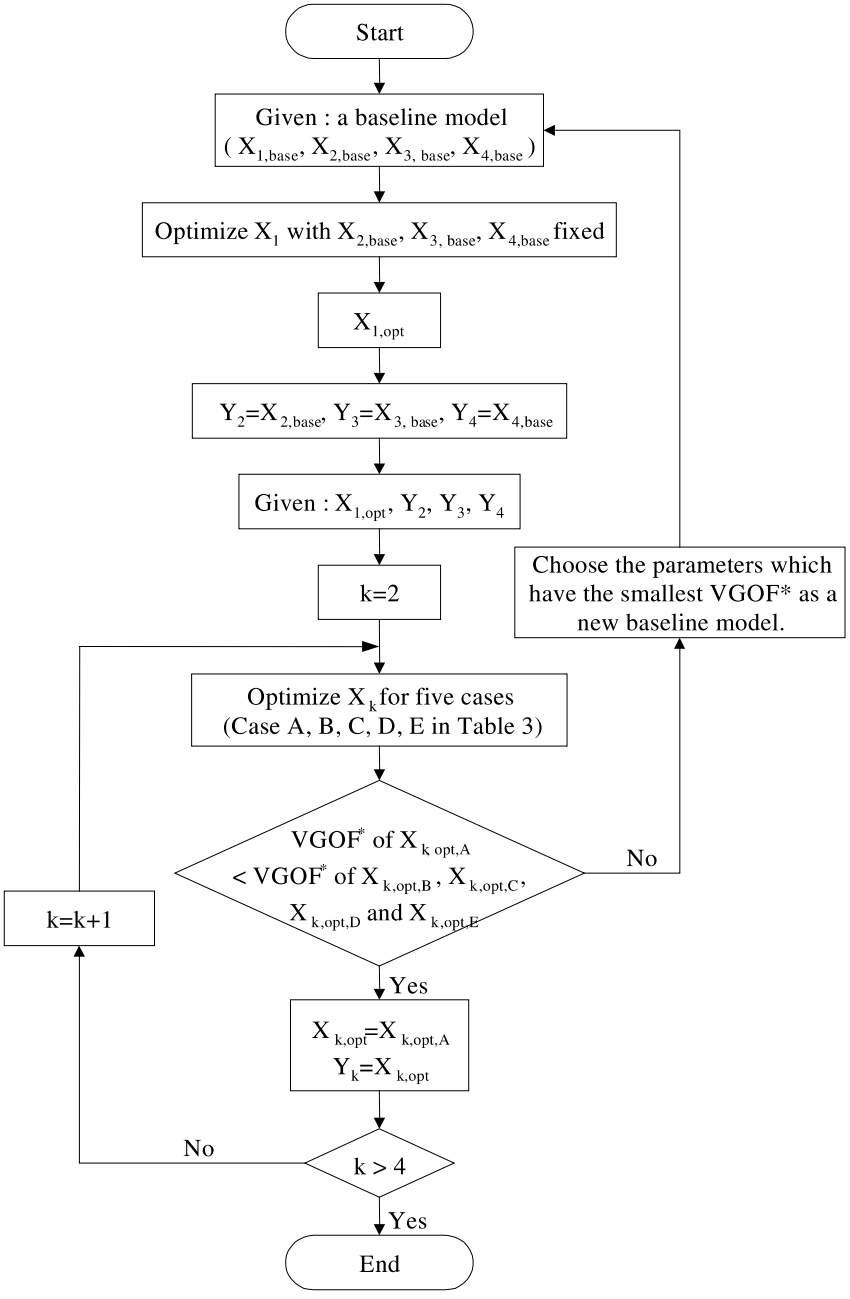

Fig. 10. The flow chart of optimization procedure ($X_1 = \mathbf{L}, X_2 = \mathbf{V}, X_3 = \boldsymbol{\beta}$ and $X_4 = \mathbf{G}$, VGOF*: the value of global objective function).

Table 3
The parameters for five cases

	To obtain $\mathbf{V}_{opt}$	To obtain $\boldsymbol{\beta}_{opt}$	To obtain $\mathbf{G}_{opt}$
Case A (original case)	$\mathbf{L}_{opt}, \boldsymbol{\beta}_{base}, \mathbf{G}_{base}$	$\mathbf{L}_{opt}, \mathbf{V}_{opt}, \mathbf{G}_{base}$	$\mathbf{L}_{opt}, \mathbf{V}_{opt}, \boldsymbol{\beta}_{opt}$
Case B	$\mathbf{L}_{opt}, 1.3 \times \boldsymbol{\beta}_{base}, \mathbf{G}_{base}$	$\mathbf{L}_{opt}, 1.3 \times \mathbf{V}_{opt}, \mathbf{G}_{base}$	$\mathbf{L}_{opt}, 1.3 \times \mathbf{V}_{opt}, \boldsymbol{\beta}_{opt}$
Case C	$\mathbf{L}_{opt}, 0.7 \times \boldsymbol{\beta}_{base}, \mathbf{G}_{base}$	$\mathbf{L}_{opt}, 0.7 \times \mathbf{V}_{opt}, \mathbf{G}_{base}$	$\mathbf{L}_{opt}, 0.7 \times \mathbf{V}_{opt}, \boldsymbol{\beta}_{opt}$
Case D	$\mathbf{L}_{opt}, \boldsymbol{\beta}_{base}, 1.2 \times \mathbf{G}_{base}$	$\mathbf{L}_{opt}, 1.3 \times \mathbf{V}_{opt}, 1.2 \times \mathbf{G}_{base}$	$\mathbf{L}_{opt}, 1.3 \times \mathbf{V}_{opt}, 1.3 \times \boldsymbol{\beta}_{opt}$
Case E	$\mathbf{L}_{opt}, \boldsymbol{\beta}_{base}, 0.8 \times \mathbf{G}_{base}$	$\mathbf{L}_{opt}, 1.3 \times \mathbf{V}_{opt}, 0.8 \times \mathbf{G}_{base}$	$\mathbf{L}_{opt}, 1.3 \times \mathbf{V}_{opt}, 0.7 \times \boldsymbol{\beta}_{opt}$

Table 4
The optimum values of each parameter

Parameters	Values
L	0.272
V	0.106
β	0.44
G	0.195

Table 5
The comparison of the friction factor and Nusselt number between optimum model and baseline model

	$fRe/(fRe)_0$	Nu/Nu_0
Optimum model	7.011	7.297
Baseline model	5.275	2.225

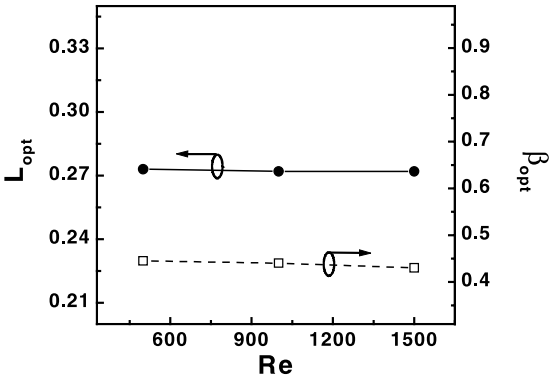

Fig. 11. $\mathbf{L}_{opt}$ and $\boldsymbol{\beta}_{opt}$ vs Reynolds number.

6. Conclusions

In this study, the thermal and flow performance in the channel of a plate heat exchanger with pins has been performed and the geometric parameters of the pin have been optimized. The global objective function determined from the correlation between the friction factor and the Nusselt number is minimized to optimize the thermal performance. The order of importance among the parameters considered is found to be in the order of **L**, **V**, **β** and **G**. Their optimum values are: $\mathbf{L} = 0.272$, $\mathbf{V} = 0.106$, $\boldsymbol{\beta} = 0.44$ and $\mathbf{G} = 0.195$. It is found that the heat transfer enhancement and pressure drop of the optimum model are increased by approximately 227.9% and 32.9%, respectively, compared with those of the baseline model. The results also indicate that the optimum geometric parameters obtained in the present study can be applied for a Reynolds number ranging from 500 to 1500 without any significant error.

Acknowledgements

One of the authors (Dr. Kwan-Soo Lee) wishes to acknowledge the financial support of the Center for Innovative Design Optimization Technology (iDOT), Korea Science and Engineering Foundation (KOSEF) and the Brain Korea 21 Project.

References

[1] D. Choudhury, K.C. Karki, Calculation of fully developed flow and heat transfer in streamwise-periodic dimpled channels, J. Thermophys. 5 (1) (1991) 81–88.
[2] T. Ohara, T. Yamamoto, H. Fujita, Evaporative heat transfer and pressure drop in a rib-roughened flat channel (effects of height and spacing of repeated transverse rib roughness), ASME/JSME Thermal Eng. Proc. 4 (1991) 399–406.
[3] A.J. Fowler, G.A. Ledezma, A. Bejan, Optimal geometric arrangement of staggered plates in forced convection, Int. J. Heat Mass Transfer 40 (8) (1997) 1795–1805.
[4] A. Bejan, in: Entropy Generation through Heat and Fluid Flow, Wiley, New York, 1982.
[5] J.Y. Yun, K.S. Lee, Influence of design parameters on the heat transfer and flow friction characteristics of heat exchanger with slit fins, Int. J. Heat Mass Transfer 43 (14) (2000) 2529–2539.
[6] A. Bejan, E. Sciubba, The optimal spacing of parallel plates cooled by forced convection, Int. J. Heat Mass Transfer 35 (12) (1992) 3259–3264.
[7] S.V. Patankar, C.H. Liu, E.M. Sparrow, Fully developed flow and heat transfer in ducts having streamwise-periodic variations of cross-sectional area, J. Heat Transfer 99 (1977) 180–186.
[8] R.H. Bravo, A. Sanchez, C.J. Chen, T.F. Smith, Convection and radiation heat transfer analysis in three-dimensional arrays of electronic components, in: InterSociety Conference on Thermal Phenomena (1992) 149–154.
[9] S.V. Patankar, in: Numerical Heat Transfer and Fluid Flow, McGraw-Hill, New York, 1980.
[10] G. de Vahl Davis, G.D. Mallinson, False diffusion in numerical fluid mechanics, School of Mech. and Ind. Eng. Rept. /FMT/1, University of New South Wales, 1972.
[11] F.P. Incropera, D.P. DeWitt, in: Introduction to Heat Transfer, third ed., Wiley, New York, 1996.
[12] S.R. Singiresu, in: Engineering Optimization (Theory and Practice), third ed., Wiley, New York, 1996.